Pre-Event Two-Stage Proactive Control for Enhanced Distribution System Resiliency

SUBIR MAJUMDER[1], (Member, IEEE), GOWTHAM KANDAPERUMAL[2], (Member, IEEE), SHIKHAR PANDEY[2], (Member, IEEE), ANURAG K. SRIVASTAVA[1], (Fellow, IEEE), AND CLAY KOPLIN[3], (Member, IEEE)

[1]Lane Department of Computer Science and Electrical Engineering, West Virginia University, Morgantown, WV 26506, USA
[2]ComEd, Chicago, IL 60181, USA
[3]Cordova Electric Cooperative (CEC), Cordova, AK 99574, USA

Corresponding authors: Anurag K. Srivastava (anurag.srivastava@mail.wvu.edu) and Subir Majumder (subir.majumder@mail.wvu.edu)

This work was supported in part by the U.S. Department of Energy Resilient Alaskan Distribution system Improvements using Automation, Network analysis, Control, and Energy Storage (RADIANCE) and U.S.-India collAborative for smart diStribution System wIth STorage (UI-ASSIST) Project under Grant DE-IA0000025.

ABSTRACT Recent advancements in prediction technologies have motivated the power distribution utilities to actively utilize forecasts to minimize the impact of high-impact low frequency (HILF) events. Accurate forecasting coupled with past operational experiences potentially enables pre-event control, aiming to reduce the impact on the system in a network with finitely large numbers of automatic and manually operated control devices. Impacts to the critical infrastructure facilities, also known as critical loads (CLs), are minimized when a section of the network is appropriately deenergized before the event strikes. However, predictions are not perfect, and given limited accuracy with ever-changing weather forecasts, control actions are required to be constantly updated until the event has passed. Once the events are predicted with high enough confidence and the necessary reconfiguration strategy has been identified, the operator must configure the manually operable switches significantly ahead of event landfall to ensure the operational crews' safe return from potentially hazardous zones. Given limited resource availability and requisite manual switching operations, some of the loads would also have to be deenergized. Overall resiliency of the system will be improved if the loads remain connected through remotely operable switches until minutes before the event makes landfall. The proposed two-stage control framework with a necessary mathematical formulation facilitates the same. Furthermore, the proposed framework enables continuous corrective action based on available lead time. The developed proactive control framework is demonstrated using a modified IEEE 123-Node system model and a real-world isolated μ-grid based on the Cordova Electric Cooperative system with superior performance results.

INDEX TERMS Critical loads, distribution system resiliency, extreme events, optimization, proactive restoration.

NOMENCLATURE

Selected set of parameters and variables are given below:

A. SETS

i, j	Indices representing nodes.
f	Index representing substation nodes.
t	Index representing various intervals.
B	Set of all nodes in network.
B^f	Set of nodes that are predicted to remain healthy.
B^F	Set of all substation nodes.
B'	Set of all nodes that remain disconnected in the post-disaster network.
W	Set of all distribution lines.
T	Set of all intervals.
$\mathbb{F}$	Set of nodes facing the catastrophe.

B. PARAMETERS

λ_i	Outage forecast indicator of node i.
$x_{i,j}$	Connectivity of permanent lines nodes i and j respectively in the typical distribution network.

$\hat{x}_{i,j}, \hat{y}_{i,j}$ Revised connectivity of permanent lines and switches between nodes i and j respectively after solving stage 1 of the optimization problem.

$S^{L}_{i,j}$ Power flow limit between nodes i and j.

$P^{CL,t}_{i}$ Active power critical load demand at node i during interval t.

$Q^{CL,t}_{i}$ Reactive power critical load demand at node i during interval t.

$P^{NCL,t}_{i}$ Active power non-critical load demand at node i during interval t.

$Q^{NCL,t}_{i}$ Reactive power non-critical load demand at node i during interval t.

$\overline{P^{DG}_{i}}, \underline{P^{DG}_{i}}$ Aggregated active power generation limits from diesel generator at node i.

$\overline{Q^{DG}_{i}}, \underline{Q^{DG}_{i}}$ Aggregated reactive power generation limits from diesel generator at node i.

$P^{F,t}_{i}, Q^{F,t}_{i}$ Scheduled injection from substation at node i during interval t.

$\underline{RR^{DG}_{i}}, \overline{RR^{DG}_{i}}$ Ramping capabilities of the diesel generator at node i.

S^{DG}_{i} Apparent power limit of diesel generator connected at node i.

M A large positive real number as a pert of big-M method.

$R_{i,j}, X_{i,j}$ Resistance and reactance of lines connected between nodes i and j respectively in the typical distribution network.

S^{BSD}_{i} Apparent power limit of battery storage device connected at node i.

$\mathcal{K}$ Interval parameter to calculate state of charge within battery.

η_{ch}, η_{dch} Charging and discharging efficiencies of battery storage devices.

$\underline{\mathrm{SOC}_i}, \overline{\mathrm{SOC}_i}$ State of the charge limits of the battery connected at node i.

k^{VL}_{i}, k^{NCL}_{i} Value of connected critical and non-critical loads at node i.

$\underline{v_i}, \overline{v_i}$ Lower and upper limit of voltages at node i.

v^{ref} Reference voltage at controlled nodes.

C. VARIABLES

$z_{i,j}$ Directed connectivity between nodes i and j without isolating the disconnected nodes.

λ_i Connectivity of node i in the post-disaster partly disconnected distribution network.

$\psi_{i,j}$ Directed connectivity between nodes i and j after isolating the nodes in the post-disaster network.

$p^{t}_{i,j}, q^{t}_{i,j}$ Active and reactive power flow between nodes i and j within interval t in the post-disaster network.

$y^{M}_{i,j}, y^{R}_{i,j}$ Connectivity of manual and remotely operable switches between nodes i and j respectively in the typical distribution network.

$P^{DG,t}_{i}$ Active power injection from diesel generator connected at node i during interval t in the post-disaster network.

$Q^{DG,t}_{i}$ Reactive power injection from diesel generator connected at node i during interval t in the post-disaster network.

$P^{BSD,t}_{i}$ Active power injection from battery storage device connected at node i during interval t in the post-disaster network.

$Q^{BSD,t}_{i}$ Reactive power injection from battery storage device connected at node i during interval t in the post-disaster network.

$P^{F,t}_{i}, Q^{F,t}_{i}$ Active and reactive power injection from the feeder during interval t.

V_i Variable to denote radiality of the post-disaster PDS.

$\alpha^{t}_{i}, \beta^{t}_{i}$ Connectivity of critical and non-critical loads at node i during interval t in the post-disaster network.

Φ^{DG}_{i} Operating status of diesel generator at node i.

v^{t}_{i} Squared nodal voltage at node i during interval t in the post-disaster network.

$\delta_{i,t}$ Charging and discharging status of the battery storage device connected at node i during interval t in the post-disaster network.

SOC^{t}_{i} The state of charge of the battery storage device connected at node i during interval t in the post-disaster network.

$\hat{(\cdot)}$ Associated second stage variables.

$(\cdot)^*$ Optimal solutions obtained with solving Stage 1 of the optimization problem.

I. INTRODUCTION

Recent studies indicate that extreme weather high-impact low frequency (HILF) events are becoming more frequent and severe, with substantial damage to the power grid [1], one of the critical infrastructures of the modern society. Once the extreme event makes landfall, the available generation from the transmission grid often gets significantly reduced [2], forcing the power distribution systems (PDS) to operate with limited generating resources, if there are any. PDS may also need to operate as an islanded μ-grid for a flexible pre-, and post-HILF event operation [3]. Various controllers and relays, some of which are equipped with autosynchronizers, facilitate seamless μ-grids operation of a part of the PDS [4], [5]. Available distributed generation facilities, such as diesel generators (DGs), battery storage devices (BSDs), and distributed energy resources (DERs), ensure resource sufficiency in μ-grids or the PDS as a whole. Furthermore, in a resource-constrained scenario, non-essential facilities need to be shed through advanced metering infrastructure (AMI), or the entire feeder can be dropped. Reclosers, sectionalizers, and various other switches at strategic grid edges can help us achieve the requisite grid flexibility by proactively creating alternative paths to critical infrastructure facilities, also called

critical loads (CLs), such as Hospitals, Police Stations, Fire Stations, and other infrastructure (see [6] for a detailed definition) in the wake of disasters. Such a prioritization ensures supply continuity or minimization of the outage duration for the CLs, improving overall resiliency of the society.

The impact of HILF events will be significantly reduced if the PDS is sufficiently prepared using early warning and prediction. Given recent advancements in short-term prediction accuracy of weather models, utilities across the USA are actively developing techniques for HILF early-warning, and forecasting impact on the power infrastructure [7] to improve their resiliency considerably. The use of machine learning (ML)-based node and line outage predictors is notable in the literature [8]–[10]. High-performance sensor deployment, data acquisition, processing technology [11], the needed information and communication technology (ICTs), along with, available rich historical event data [12] can significantly help in the development of the predictive models, as well as, judicious deployment of control actions for improving power system resiliency.

Multiple proactive PDS resiliency improvement strategies are reported in the literature. These include topics such as proactive crew mobilization for optimal post-disaster PDS restoration [13], pre-event diesel fuel and battery (in the form of electric buses) allocation [14], generator re-dispatch, topology switching [15], proactive resource sufficiency facilitating μ-grid operation [16], and proactive charging of BSDs for successful in-event μ-grid operation [17] for reference. Additionally, related literature that considers sequential re-dispatch of DGs [18], dynamic line rating based on probabilistic scenario generation [19], island formation based on Monte-Carlo simulation [20], data mining approaches for an iterative load shift-and-shed [21], are notable. While robust optimal solutions are majorly used in the existing literature to ensure grid survival even in the wake of a worst-case uncertainty, they perform poorly in the best-case scenario, especially when the HILF events continuously evolve and can entirely disappear as time progresses. With increasing investment in HILF forecasting by the utilities, a forecast-driven methodology for resiliency improvement gains immense significance. Furthermore, given the availability of various switches within the grid, PDS reconfiguration and resource allocation in the wake of a disaster would be challenging.

Keeping the PDS energized while the HILF event is in progress would cause safety hazards to both civilians and operational or repair crews (reference [22] reported in-event injury of firefighting crew due to contact with the grounded energized power lines). Damaged energized infrastructure can also be a source of secondary hazards (notably, public safety power shut-off, PSPS, events in California, USA is developed to minimize secondary hazard risk [23]) and can delay post-disaster recovery in some scenarios (as reported by CEC, pre-event generator shut down before tsunami or snow avalanche is necessary to expedite restoration). In the same line, the focus of this work is to selectively deenergize a part of the network before the disaster strike while minimizing its impact on the critical infrastructures to reduce its impact on humanity. The existence of manually operable (MO) [11] switches alongside automated/remotely operable (RO) ones within the PDS necessitates deployment of the operational crew for the necessary reconfiguration. Operations crews need to be dispatched with sufficient lead time to ensure their safe return from the hazardous zone.[1] The crew executes network reconfiguration utilizing coordinated operation of MO and RO switches while ensuring maximal survival of CLs through reconfiguration and proactive de-energization. Furthermore, predicting HILF events can be challenging, and the forecasts can change rapidly. Therefore, as HILF events approach, crews should no longer remain deployed but instead evacuate for safety concerns.

We observe four seemingly counterposed challenges in the development of the proactive control strategy: (i) PDS operators (DSOs) will rely on HILF forecasts for the proactive control, (ii) the outage prediction accuracy with HILF events can deviate significantly in a longer temporal horizon [24], (iii) allowable lead-time in operational crew-dispatch, and (iv) prior de-energization of the part of PDS, although needed, will cause inconvenience for the civilians. Prior de-energization can be misapplied or over-applied if the event significantly deviates from the early forecasts. The proposed two-stage proactive control framework that references forecast revisions to reconfigure the system for an enhanced PDS-wide resiliency helps circumvent these issues. Here, instead of completely de-energizing a part of the PDS hours before to ascertain safe dispatch and return of the operational crews, we ensure the disastrous part of the PDS remains connected through RO switches. This strategy helps us keep a section of the PDS energized hoping that the HILF event will clear itself while also increasing topological resilience of the system. Hours-ahead crew deployment for the reconfiguration of MO switches coordinated by RO switch operations would facilitate the same.

Furthermore, the network will be so configured that this disastrous area will be isolated at the last possible minute of the disaster landfall through RO switches. The requisite switching operation will be proactively modified based on the available forecast until the disaster strikes. Compared to the ones discussed in the literature review, this paper considers the availability of multiple different switches in the PDS and requisite crew dispatch to facilitate the operation of MO switches within the network with the associated timeline. The proposed framework would also encourage utilities to study and plan for various ways a disaster may materialize before an event and devise suitable control actions. Some of the loads outside of the hazardous zone may experience de-energization, while other portions of the PDS may operate as μ-grids to maximize the survival of CLs. These scenarios add complexity requiring advancement of the reconfiguration

[1] Entire PDS can become a hazardous zone during a disaster. Discussed ML-based techniques could identify specific regions of outage depending on system conditions, weather intensity, etc.

methodology presented in [25]. Operation of the network as the disaster is in progress [26], or for restoration [27] is beyond the scope of this work.

The contribution of this paper is, therefore, threefold:

(i) Proposed a novel two-stage proactive network-switching and resource allocation strategy that maximizes PDS CL survivability, capable of utilizing HILF early warning and outage prediction, and considers the availability of various switches. Here, coordinated MO and RO switch operations are deployed hours before by the operational crews to ensure crew safety requirements, while a part of the PDS infrastructures will be deenergized minutes before the disaster makes a landfall. These hours- and minutes-ahead operations will be coordinated appropriately, with hours-ahead operations constantly updated based on revised forecasts and suitably deployed depending on available lead time for the operational crew.

(ii) Developed a new mathematical formulation for isolating possible outage zones from healthy zones, forming μ-grids while preserving radial operability, with a detailed mathematical guarantee. The proposed formulation considers the condition where the entire PDS must be separated into multiple μ-grids, with each one connected to a separate substation, or if transmission as the whole network is suffering from an outage.

(iii) Developed a resiliency metric-driven performance analysis tool based on our previous research and used it to validate the proposed algorithm utilizing the modified IEEE 123-node test system and a real-world 45-node μ-grid based on the CEC grid. We show that the performance analysis tool could be used as an advisory to the DSO, who could consider and contextualize the strategy before deploying it, and is even suitable for any progressing weather events. A practical framework has been developed in this regard to facilitate the same. Given the limited operating time horizon for the DSO, the Decision Support (DS) tool will provide the DSO with the reconfiguration strategy. The performance analysis tool will identify the potential impact on the PDS with and without deployment of the reconfiguration strategy for the operating time horizon. The situational awareness (SA) tool would involve forecasted progress of the HILF event, its impact on the PDS, and early warning signals.

The rest of the paper is organized as follows. The Problem Statement that formalizes the mathematical model of the two-stage optimization problem is introduced in Section II. In Section III, a solution framework showing both situational awareness and decision support to the DSO is outlined. A Numerical Analysis that contrasts the impact of both contemporary and proposed response strategies on a hypothetical and a real-world network is presented in section IV, and the Conclusion is summarized in Section V.

II. PROBLEM STATEMENT

While a majority portion or all of a PDS can fall within the hazardous zone during a disaster, only a finite set of nodes will ultimately face catastrophe and subsequent outage. Such nodes were previously captured using fragility curve [20]. Limited availability of switches across the PDS may extend the impacts to additional lines and nodes. The corresponding set of nodes can be called nodes with expected outages (NwEO). Availability of switches can significantly reduce the scope of the NwEO, but MO switches, such as manually operated loadbreak switches, severely limit their deployment. Proactive control facilitates PDS reconfiguration minimizing NwEO and assuring the survival of the maximum number of CLs. Proactive control also enables connectivity of the CLs within the NwEO until the last minute of the appearance of the disaster. Forecast-driven approaches can significantly reduce the computational requirements compared to probabilistic methods, and utilities are actively investing in HILF forecasts, which motivates us to use HILF forecasts in developing proactive measures. However, given the associated volatility, the network must be continuously reconfigured if the NwEO gets updated with a sufficiently high confidence interval (CI). The NwEO must also remain connected before HILF makes landfall so that the associated CLs will not face any deenergization if the threat is eliminated and facilitate successive reconfiguration, if needed, improving PDS resiliency.

As previously indicated, the analysis begins with an early warning of the HILF scenario followed by its forecasted progress, characterizing the impact timeline of the disaster on the PDS. HILF-oriented load and generation forecasts can be a part of DSO's Advanced Distribution Management System (ADMS). As peovided in Fig. 1,[2] the proposed resiliency management system (RMS) can be a part of the ADMS. HILF forecasting is not within the scope of this paper and is considered to be given. Based on the forecast, the RMS tool analyzes estimated threats on the PDS, and the DS tool within the RMS identifies a reconfiguration strategy to maximize the survivability of the CLs and associated deployment timeline. The performance analysis tool within the RMS provides the DSO with a resiliency metric indicating forecasted impact on the PDS, with the metric improvement following the deployment of the proposed reconfiguration strategy. Notably, the reconfiguration will be necessary if the HILF with a high CI falls within DSO observable time horizon. The operator will also be provided with several landmark events, including early-warning and associated impact on the PDS and landfall of the weather events as SA measures. Furthermore, the RMS relies on DSO to properly deploy suggested reconfiguration action.

As discussed in [28], given the objective is to ensure the survival of the CLs until the last minute of disaster landfall while also being constrained by the operation of MO

[2]Wildfire topographical imagery in Fig. 1 as a part of HILF event progress are taken from: https://cimss.ssec.wisc.edu/satellite-blog/archives/34786

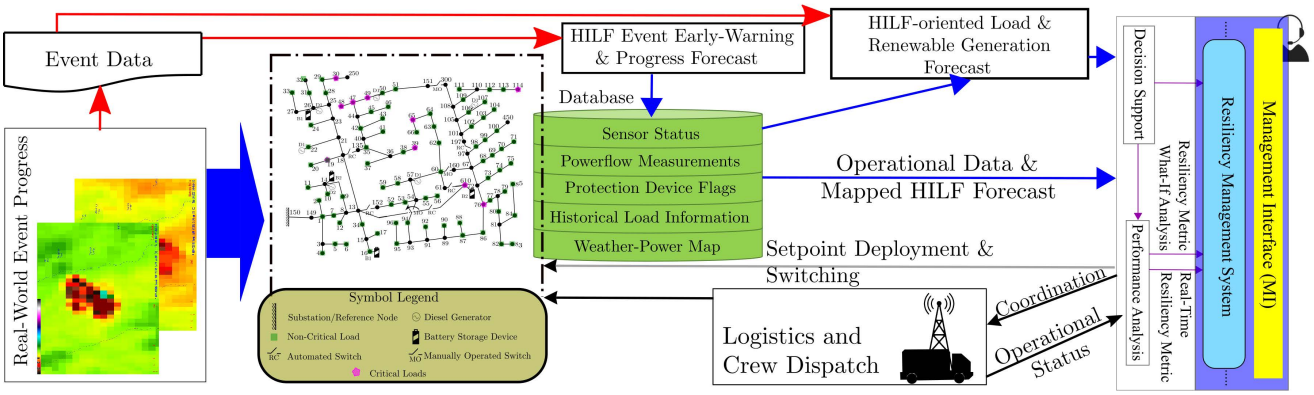

FIGURE 1. **Overall architecture of the proposed two-stage proactive control for distribution system resiliency.**

switches, we propose a two-pronged approach. In the first stage, we identify minimal possible NwEO through reconfiguring both RO and MO switches and the necessary set points for the DERs. The timeline of the switching deployment will be a function of available time prior to disaster landfall and lead time for crew deployment to maximize overall resiliency. Depending on the available relays and DGs, multiple μ-grids can also be formed in this process. Given the solution of stage 1, the second stage involves computation of RO switching operations and resource provision needed to keep an optimal subset of NwEO connected with the healthy part (or remain energized as μ-grids) until minutes before the event materializes. This connectivity ensures reduced switching requirements if the network must be reconfigured again while improving the system's topological resilience. It is trivial that switching actions in both stages are mutually exclusive, and combined deployment of the switching strategy would ensure the survival of CLs until the last minutes of disaster landfall. Requisite crew dispatch would require us to deploy this hours ahead (HA). Furthermore, closed remote switches, determined in the second stage, are opened as a part of the minutes-ahead operation (MA) before the disaster strikes to de-energize NwEO. Therefore, although the problem structure of HA and MA operations would be similar, their differences would be captured due to their different timeline of deployment. Notably, local generators within the NwEO will also be disconnected as part of anti-islanding protection in the MA operation. Without loss of generality, we also assume that the loads are aggregated at each node and controllable through AMI switches. The detailed deployment algorithm will be discussed later in this paper. Please note that in-event voltage and frequency control is beyond the scope of this paper.

The mathematical framework for both stages of the optimization problem is outlined in the following subsections:

A. STAGE 1: PRO-ACTIVE DECISION MAKING WITH ISOLATION OF NwEO

In any emergency plan, it is important to capture critical infrastructure co-dependency [29]. In an extreme resource-constrained scenario, especially when a HILF event is in progress, some of the loads will be required to be shedded, and the relative criticality could be used to maximize societal resiliency. In this paper, the relative importance of the CLs and non-critical loads (NCLs) are given by factors k_i^{CL} and k_i^{NCL} respectively (where, $k_i^{CL} \gg k_i^{NCL}$), with the objective function being the maximization of the value of the served load. Consideration of such a definition for resiliency improvement is well documented in the literature [30]. We assume that CLs and their non-critical counterpart in the distributor are separable via AMI switches, and their availability is identified using α_i^t and β_i^t, respectively. Additionally, $P_i^{CL,t}$ and $P_i^{NCL,t}$ are active power demand of CL and NCLs, respectively. We identify the NwEO through the integer variable λ_i ($\in \{1, 2\}$). Here, $\lambda_i = 1$ symbolizes that a node remains energized, and $\lambda_i = 2$ otherwise. Consequently, the objective function becomes:

$$\max \sum_{\forall t \in T} \sum_{\forall i \in B} k_i^{CL} \alpha_i^t (2 - \lambda_i) P_i^{CL,t} + k_i^{NCL} \beta_i^t (2 - \lambda_i) P_i^{NCL,t} \tag{1}$$

Here, the optimization problem is solved for a pre-defined temporal event horizon (identifying the DSO observable time horizon). The constraint set for the switching and resource allocation problem is divided into four parts as follows: (i) radiality of the PDS, (ii) connectedness of the nodes, (iii) power flow equations, and (iv) constraints pertaining to the BSDs.

1) CONSTRAINTS TO ENSURE RADIALITY

To derive the resulting radial network isolating NwEO, we extend the formulation given in [31]. Suppose W be the set of all the branches/lines and B ($i, j \in B$) be the set of nodes in the PDS. Each $x_{i,j} = 1$ represent a permanent line. A line can have a MO or RO switch, identified by, $y_{i,j}^M \in \{0, 1\}$, and $y_{i,j}^R \in \{0, 1\}$, respectively. Consequently, $0 \leq x_{i,j} + y_{i,j}^M + y_{i,j}^R \leq 1$ for each of the node-pairs. To ensure radiality, we obtain a directed tree utilizing the variable $z_{i,j}$, where, if a branch is directed from node i to node j, then, $z_{i,j} = 1$ and $z_{j,i} = 0$, otherwise. Furthermore, the direction of

the branches emanating from the root node, representing the substation, f ($\in B^F$), is always away from it, or $z_{i,f} = 0$. This produces the following set of equations:

$$z_{i,j} \in \{0, 1\}; \quad \forall i, j \in B \tag{2}$$

$$z_{i,j} + z_{j,i} = x_{i,j} + y^M_{i,j} + y^R_{i,j}; \quad \forall i, j \in B \tag{3}$$

$$z_{i,f} = 0; \quad \forall i \in B^F \tag{4}$$

Consequently, if the resulting graph remains connected, then, $\sum_{\forall j:(i,j)\in W} z_{j,i} = 1$ at every node except the substation. In the current scenario, the operation of switches to isolate NwEO will lead to multiple disconnected graphs. We must therefore need to consider a degenerated version of the condition given as:

$$\sum_{\forall j:(i,j)\in W} z_{j,i} \leq 1; \quad \forall i \in B \tag{5}$$

However, as discussed in [25], the formation of a loop remains unhindered. We utilize the following constraint to ensure radiality for each of the disjoint graphs:

$$z_{i,j}\left(V_i - V_j + \epsilon\right) = 0; \quad \forall i, j \in B \text{ and } \epsilon > 0 \tag{6}$$

Lemma 1: For each connected cluster, there will be precisely one node with a maximum value of V_i.

Proof: We will prove this by contradiction. Suppose there exist two nodes with similar V_i, which is higher than the rest of the V_i within the connected graph. Let us name these two nodes as j and k. Since, $V_j = V_k$, those two nodes cannot have a common edge (see, (6)). Suppose, the associated directed edges are $j \to m$, and $k \to n$ (directions satisfy (6), directedness arises from (3)). If, m and n identifies the same node, then, condition (5) will be violated. If, nodes m and n are connected, without the loss of generality, suppose that $m \to n$, and consequently, condition (5) will be violated at node n. Otherwise, we can suppose that $V_m = V_n$, and are not directly connected. Without loss of generality, we can recursively prove that there will be a node or edge, where either of the conditions (2) - (6) will be violated. This proof can be easily extended for three or more nodes. □

Theorem 1: The node with maximum V_i for each connected cluster will have $\sum_{\forall j:(i,j)\in W} z_{j,i} = 0$.

Proof: From Lemma 1, the uniqueness of the node i with highest V_i signifies all the edges are directed away from it (see, (3) and (6)). And consequently, $\sum_{\forall j:(i,j)\in W} z_{j,i} = 0$, at that particular node. Now, to prove the exactness, let us consider a connected sub-graph of the cluster containing the node i, with the highest V_i, and the rest of the nodes with exactly one branch incident on it. Suppose j is one such arbitrarily chosen node. Also, suppose, G_m be another sub-graph with a node m, with $\sum_{\forall n:(m,n)\in W} z_{n,m} = 0$, and rest of the nodes with exactly one branch incident. Now, if m is connected to j, and, $m \to j$ (5) is violated. If $j \to m$, then both the subgraphs are connected with the requisite condition satisfied only at node i. Also, $m \to i$ is infeasible by definition. This proves the uniqueness. □

Corollary 1: Condition (2)*,* (3)*,* (5) *and* (6) *upholds radiality for a connected graph.*

Proof: Since the graph is connected, from Theorem 1, there will be precisely one node with all the edges are directed away from it. The connected graph's radiality under such a condition is already proven in [31]. □

Remark 1: Equations (2)-(5)*, along with* (6) *ensure radiality of each of the part of the reconfigured part. Condition* (4) *enforces that the substation node will have $\sum_{\forall j:(i,j)\in W} z_{j,i} = 0$. However, the resulting graph can still be disconnected. Each of the disconnected cluster will have precisely one node with $\sum_{\forall j:(i,j)\in W} z_{j,i} = 0$. We can designate this node as μ-grid central voltage controlled node, which is similarly utilized in the latter part of the paper.*

2) CONSTRAINTS TO ENSURE CONNECTEDNESS OF THE NODES

Parameter $\bar{\lambda}_i$ identifies whether node i will face outages, and is defined as follows:

$$\bar{\lambda}_i = \begin{cases} 2, & \forall i \in \mathbb{F} \\ 1, & \forall i \in B^f \\ 0, & \forall i \in B \setminus \left(B^f \cup \mathbb{F}\right) \end{cases} \tag{7}$$

Here, $\mathbb{F}$ is the set of nodes facing catastrophe. B^f is the set of nodes that are predicted to remain healthy. As for the undetermined set of nodes, as given in (10), it is trivial that if any two adjacent nodes are connected ($x_{i,j} + y^M_{i,j} + y^R_{i,j} = 1$), then $\lambda_i = \lambda_j$. Notably, the values of λ_i are independent of the direction of the directed rooted tree indicated by $z_{i,j}$. The outage information is expected to be provided by the HILF forecaster. The energization status of the nodes relies on the predicted HILF scenario and is given in (9).

$$\lambda_i \in \{1, 2\}; \quad \forall i \in B \tag{8}$$

$$\lambda_i \geq \bar{\lambda}_i; \quad \forall i \in B \tag{9}$$

$$\left(\lambda_i - \lambda_j\right)\left(x_{i,j} + y^M_{i,j} + y^R_{i,j}\right) = 0; \quad \forall (i,j) \in W \tag{10}$$

Remark 2: Only the energized section of the network will have $\lambda_i = 1$.

Proof: As determined by, $x_{i,j} + y^M_{i,j} + y^R_{i,j}$, if an edge between nodes i and j exists, then, from (10), $\lambda_i = \lambda_j$. Therefore, given expected HILF scenario indicated by $\hat{\lambda}_i$, all the NwEO will have $\lambda_i = 2$. The connectivity of switches determines the value of λ_i for adjacent nodes. As for the rest of the nodes, associated λ_i are driven by the objective function. Our objective function is equivalent to, maximization of the weighted sum of $(2 - \lambda_i)$, which indirectly enforces $\lambda_i = 1$ for the energized counterpart. □

Now, we have to identify directed clusters containing only the energized part of the PDS (identified by $\psi_{i,j}$). Let us consider a directed branch between nodes i and j. Since, $\lambda_i = 2$ at the NwEO, then for $\lambda_i + \lambda_j \geq 3$, the associated branch cannot remain energized, or, $\psi_{i,j} = \psi_{j,i} = 0$. For $\lambda_i + \lambda_j < 3$, the associated branch is retained as a healthy branch. Note that the value of $z_{i,j}\left(\lambda_i + \lambda_j - 3\right)$ is limited within $[-1, 1]$. Thus

the following set of equations are derived:

$$\psi_{i,j} \in \{0,1\}; \quad \forall (i,j) \in W \tag{11}$$

$$\psi_{i,j} \leq z_{i,j}; \quad \forall (i,j) \in W \tag{12}$$

$$z_{i,j}\left(\lambda_i + \lambda_j - 3\right) \leq (1 - \psi_{i,j}) - \epsilon\psi_{i,j}; \quad \forall (i,j) \in W \tag{13}$$

$$z_{i,j}\left(\lambda_i + \lambda_j - 3\right) \geq -\psi_{i,j}; \quad \forall (i,j) \in W \tag{14}$$

Here, (11)-(14) mathematically represent the two prior constraints as outlined. Notably, ϵ is a small positive real number that linearizes the conditional expression.

Remark 3: Equations (2)-(14) *identify the directed, healthy, and radial clusters through the operation of the necessary switches. NwEO set will be automatically isolated.*

Note that ensuring radiality and connectedness of the energized nodes does not guarantee μ-grid formation and has to be driven by the suitable relays and DGs availability. Without a μ-grid control center, the DSOs interface can still control the entire distribution grid.

3) POWER-FLOW EQUATIONS

As shown in (15)-(16), power can flow in both the directions along the path symbolized by $\psi_{i,j}$. The nodal balance equations for power flow are driven by the variable $(2-\lambda_i)$, identifying the healthy part, and is given in (17)-(18).

$$-S^L_{i,j}\psi_{i,j} \leq p^t_{i,j} \leq S^L_{i,j}\psi_{i,j}; \quad \forall (i,j) \in W, \forall t \in T \tag{15}$$

$$-S^L_{i,j}\psi_{i,j} \leq q^t_{i,j} \leq S^L_{i,j}\psi_{i,j}; \quad \forall (i,j) \in W, \forall t \in T \tag{16}$$

$$P^t_i = \alpha^t_i(2-\lambda_i)P^{CL,t}_i + \beta^t_i(2-\lambda_i)P^{NCL,t}_i - \sum_{\forall DG} P^{DG,t}_i - \sum_{\forall BSD} P^{BSD,t}_i - P^{F,t}_i; \quad \forall i \in B, \forall t \in T \tag{17}$$

$$Q^t_i = \alpha^t_i(2-\lambda_i)Q^{CL,t}_i + \beta^t_i(2-\lambda_i)Q^{NCL,t}_i - \sum_{\forall DG} Q^{DG,t}_i - \sum_{\forall BSD} Q^{BSD,t}_i - Q^{F,t}_i; \quad \forall i \in B, \forall t \in T \tag{18}$$

Here, α^t_i and β^t_i represent interval-wise connectivity status of critical and non-critical nodes ($\in \{0,1\}$). Additionally, $P^{F,t}_i$ and $Q^{F,t}_i$ are the parameters representing active and reactive power injection from the substation. Also, $P^{CL,t}_i$ and $Q^{CL,t}_i$ are forecasted active and reactive power demands of CLs, while, $P^{NCL,t}_i$ and $Q^{NCL,t}_i$ are forecasted active and reactive power demands of NCLs. Additionally, $P^{DG,t}_i$ and $Q^{DG,t}_i$ are the variables representing active and reactive power injection from the DGs. Finally, $P^{BSD,t}_i$ and $Q^{BSD,t}_i$ are the active and reactive power injection from BSDs. In (17)-(18), P^t_i and Q^t_i represent nodal extraction of active and reactive power. Also, $S^L_{i,j}$ is the line flow limit.

$$\Phi^{DG}_i \leq (2-\lambda_i); \ \forall i \in B \tag{19}$$

$$\left(P^{DG,t}_i\right)^2 + \left(Q^{DG,t}_i\right)^2 \leq \Phi^{DG}_i\left(S^{DG}_i\right)^2; \ \forall i \in B, \ \forall t \in T \tag{20}$$

$$\Phi^{DG}_i\underline{P^{DG}_i} \leq P^{DG,t}_i \leq \Phi^{DG}_i\overline{P^{DG}_i}; \ \forall i \in B, \forall t \in T \tag{21}$$

$$\Phi^{DG}_i\underline{RR^{DG}_i} \leq P^{DG,t+1}_i - P^{DG,t}_i \leq \Phi^{DG}_i\overline{RR^{DG}_i}; \quad \forall i \in B, \ \forall t \in T \tag{22}$$

$$\Phi^{DG}_i\underline{Q^{DG}_i} \leq Q^{DG,t}_i \leq \Phi^{DG}_i\overline{Q^{DG}_i}; \quad \forall i \in B, \ \forall t \in T \tag{23}$$

If a DG connected at node i remains healthy (determined by DG availability Φ^{DG}_i and nodal energization status), active and reactive power injection will be limited by its capability curve (20)-(23). Here, S^{DG}_i is the rating of DGs. Furthermore, $\underline{P^{DG}_i}$, $\overline{P^{DG}_i}$ are lower and upper limits of active power generation, respectively, from DGs, if operational. Similarly, $\underline{Q^{DG}_i}$, $\overline{Q^{DG}_i}$ are lower and upper limits of reactive power generation, respectively. Also, $\underline{RR^{DG}_i}$, $\overline{RR^{DG}_i}$ identifies ramping capabilities of the DGs.

Given the nodal node injections, the line-flow equations (active and reactive power line flow being $p^t_{i,j}$ and $q^t_{i,j}$ respectively) as a part of the linearized dist-flow equations [32] are given by:

$$\sum_{\forall j:(i,j)\in W} p^t_{j,i} - p^t_{i,j} = P^t_i; \quad \forall i \in B, \ \forall t \in T \tag{24}$$

$$\sum_{\forall j:(i,j)\in W} q^t_{j,i} - q^t_{i,j} = Q^t_i; \quad \forall i \in B, \ \forall t \in T \tag{25}$$

$$\left(p^t_{i,j}\right)^2 + \left(q_{i,j}\right)^2 \leq \left(S^L_{i,j}\right)^2; \quad \forall (i,j) \in W, \ \forall t \in T \tag{26}$$

Note that the connectivity of energized lines in (26) are indirectly accounted for in (15)-(16). For the network voltage to stay within limits while maintaining the voltage at the substation, or, μ-grid voltage-controlled node at the predetermined reference voltage, v^{ref}, the following set of equations must be satisfied:

$$v^t_i \leq v^t_j + 2\left(R_{i,j}p^t_{i,j} + X_{i,j}q^t_{i,j}\right) + M(1-\psi_{i,j}); \quad \forall (i,j) \in W, \quad \forall t \in T \tag{27}$$

$$v^t_i \geq v^t_j + 2\left(R_{i,j}p^t_{i,j} + X_{i,j}q^t_{i,j}\right) - M(1-\psi_{i,j}); \quad \forall (i,j) \in W, \quad \forall t \in T \tag{28}$$

$$-M\left(\lambda_i - 1\right) + \underline{v_i} \leq v^t_i \leq \overline{v_i} + M\left(\lambda_i - 1\right); \quad \forall i \in B, \quad \forall t \in T \tag{29}$$

$$\left(1 - \sum_{\forall j:(i,j)\in W} z_{j,i}\right)\left(v^t_i - v^{ref}\right) = 0; \quad \forall i \in B, \ \forall t \in T \tag{30}$$

Equation (30) utilizes Remark 2. Here, v^t_i refers to the squared magnitude of nodal voltages. Also, $\underline{v_i}$ and $\overline{v_i}$ are the squared nodal voltage lower and upper limits. The indicated voltage lower and upper limits remain active only at the healthy section of the PDS (note the use of $\psi_{i,j}$). This constraint is represented through the big-M method (M being a large positive real number). Additionally, $r_{i,j}$ and $x_{i,j}$ are resistances and reactances of the concerned lines.

4) CONSTRAINTS PERTAINING TO BATTERIES

Due to the finiteness of the capacity of power-electronic converter-interfaced batteries, they can support the load demand only for a limited operating horizon. BSDs are capable of operating in all four quadrants, and their capability curve is given by (31). Here, S_i^{BSD} is the ratings of BSDs.

$$\left(P_i^{BSD,t}\right)^2 + \left(Q_i^{BSD,t}\right)^2 \leq (2-\lambda_i)\left(S_i^{BSD}\right)^2; \quad \forall i \in B,\ \forall t \in T \tag{31}$$

Additionally, asymmetric charging and discharging efficiencies due to lossy batteries and converters should also reflect in the state of the charge (SOC) of the battery. Let, $\delta_i^{BSD,t}$ ($\in \{0, 1\}$) symbolizes charging and discharging status, then:

$$P_i^{BSD,t} = P_i^{BSD,t,+} - P_i^{BSD,t,-}; \quad \forall i \in B,\ \forall t \in T \tag{32}$$

$$0 \leq P_i^{BSD,t,+} \leq \delta_i^{BSD,t} S_i^{BSD}; \quad \forall i \in B,\ \forall t \in T \tag{33}$$

$$0 \leq P_i^{BSD,t,-} \leq \left(1-\delta_i^{BSD,t}\right) S_i^{BSD}; \quad \forall i \in B,\ \forall t \in T \tag{34}$$

Given the charging/discharging status, (35) is used to calculate the SOC of the batteries. As shown in (36)-(37), the operating SOC (SOC_i^t), is limited by $\underline{\text{SOC}_i}$, $\overline{\text{SOC}_i}$, and initial SOC is the parameter defining initial status, SOC_i^{ini}.

$$\text{SOC}_i^t = \text{SOC}_i^{t-1} - \mathcal{K}\left(\delta_{i,t} P_i^{BSD,t,+} \eta_{dch}^{-1} + \left(1-\delta_{i,t}\right) P_i^{BSD,t,-} \eta_{ch}\right);\ \forall i \in B,\ \forall t \in T \tag{35}$$

$$\text{SOC}_i^t \in \{\underline{\text{SOC}_i}, \overline{\text{SOC}_i}\}; \quad \forall i \in B,\ \forall t \in T \tag{36}$$

$$\text{SOC}_i^0 = \text{SOC}_i^{ini}; \quad \forall i \in B \tag{37}$$

B. STAGE 2: PROACTIVE SAFETY-CONSTRAINED SWITCHING OPERATION WITHOUT ISOLATING NwEO

The NwEO will be deenergized through RO switches if the predicted HILF scenario persists until minutes before the disaster materializes. To ensure minimal disturbances in the rest of the system upon their deenergization, we consider zero flow through the RO switches connecting NwEO. Also, the PDS topology, line-flow, load, generation, and substation injection schedule of the healthy part of the grid, as obtained using the first stage of the optimization problem, is held constant. Hence, the decision variables in Stage 2 include the switching operation to ensure connectivity of the NwEO, the switching condition of loads and DGs, and power output from DGs and batteries within NwEO to ensure local load-generation balance.

Suppose B' is the set of nodes in the healthy section of the network (with $\lambda_i^* = 1$) obtained after solving Stage 1 (described in the previous subsection). Also, for $i, j \in B'$, $\psi_{i,j}^*$ are the associated directional connectivity. Let, $\alpha_i^{t,*}$, $\beta_i^{t,*}$, $P_i^{DG,t,*}$, $P_i^{BSD,t,*}$, $p_{i,j}^{t,*}$ be the optimal connectivity status variables corresponding to CL and NCLs, power output from DGs and BSDs, and line flows obtained from Stage 1 of the problem. While, for $i, j \in B \setminus B'$, $\hat{\alpha}_i^t$, $\hat{\beta}_i^t$, $\hat{P}_i^{DG,t}$, $\hat{P}_i^{BSD,t}$, $\hat{p}_{i,j}^t$ are the associated Stage 2 variables. Determined closed switches in Stage 1 are treated as permanent lines to calculate $\hat{x}_{i,j}$, while, optimal $\hat{y}_{i,j}^R$ is calculated only for remotely operated opened switches obtained in Stage 1. Consequently, variables in first and second stage are related as follows:

$$\hat{z}_{i,j} \geq \psi_{i,j}^*; \quad \forall (i,j) \in W \tag{38}$$

$$\hat{\lambda}_i \leq \lambda_i^*; \quad \forall i \in B \tag{39}$$

$$\alpha_i^t = \alpha_i^{t,*} + (\lambda_i^* - 1)\hat{\alpha}_i^t; \quad \forall i \in B \tag{40}$$

$$\beta_i^t = \beta_i^{t,*} + (\lambda_i^* - 1)\hat{\beta}_i^t; \quad \forall i \in B \tag{41}$$

$$\hat{P}_i^{DG,t} = P_i^{DG,t,*} + (\lambda_i^* - 1)\hat{P}_i^{DG,t}; \quad \forall i \in B \tag{42}$$

$$\hat{P}_i^{BSD,t} = P_i^{BSD,t,*} + (\lambda_i^* - 1)\hat{P}_i^{BSD,t}; \quad \forall i \in B \tag{43}$$

$$\hat{Q}_i^{DG,t} = Q_i^{DG,t,*} + (\lambda_i^* - 1)\hat{Q}_i^{DG,t}; \quad \forall i \in B \tag{44}$$

$$\hat{Q}_i^{BSD,t} = Q_i^{BSD,t,*} + (\lambda_i^* - 1)\hat{Q}_i^{BSD,t}; \quad \forall i \in B \tag{45}$$

$$p_{i,j}^t = \psi_{i,j}^* p_{i,j}^{t,*} + (1-\psi_{i,j}^*)\hat{p}_{i,j}^t; \quad \forall (i,j) \in W, \forall t \in T \tag{46}$$

$$q_{i,j}^t = \psi_{i,j}^* q_{i,j}^{t,*} + (1-\psi_{i,j}^*)\hat{q}_{i,j}^t; \quad \forall (i,j) \in W,\ \forall t \in T \tag{47}$$

Connectivity of the directed subgraph obtained in Stage 1 is enforced through (38)-(39). The revised connectivity of CLs, NCLs, active and reactive power injection from DGs and batteries for the NwEO part will be controlled through $(\lambda_i^* - 1)$, and is given in (40)-(45). Revised flow will be governed by $(1 - \psi_{i,j}^*)$. Variables determined in Stage 1 will remain as it is, and, all the constraints corresponding to radiality, nodal connectivity, power flow balance equations, and constraints pertaining to the battery need to be considered. Also, as given in (48)-(49), the focus is only on the operation of remote switches.

$$\hat{z}_{i,j} + \hat{z}_{j,i} = \hat{x}_{i,j} + \hat{y}_{i,j}^R; \quad \forall i,j \in B \tag{48}$$

$$\left(\hat{\lambda}_i - \hat{\lambda}_j\right)(\hat{x}_{i,j} + \hat{y}_{i,j}^R) = 0; \quad \forall (i,j) \in W \tag{49}$$

The objective function used in the second stage remains similar to first stage, and is given by:

$$\max \sum_{\forall t \in T} \sum_{\forall i \in B'} k_i^{CL}(2-\hat{\lambda}_i)\alpha_i^t P_i^{CL,t} + k_i^{NCL}(2-\hat{\lambda}_i)\beta_i^t P_i^{NCL,t} \tag{50}$$

III. SOLUTION METHODOLOGY

A. THE PROACTIVE DECISION-MAKING FRAMEWORK

Typically grid-connected PDS is expected to operate as an islanded μ-grid as necessary. Previously discussed autosynchronizers, available switches (both RO and MO), DGs, and protection devices facilitate such an endeavor. While retail markets can exist; when it is imminent that the PDS would operate at limited capacity with a high CI due to an impending disaster, with the availability of controllable loads, DERs, and storage devices, the DSO would consider charging its BSDs to a sufficient level to minimize the impact. The operator would be alerted through the SA mechanism. Still, the system

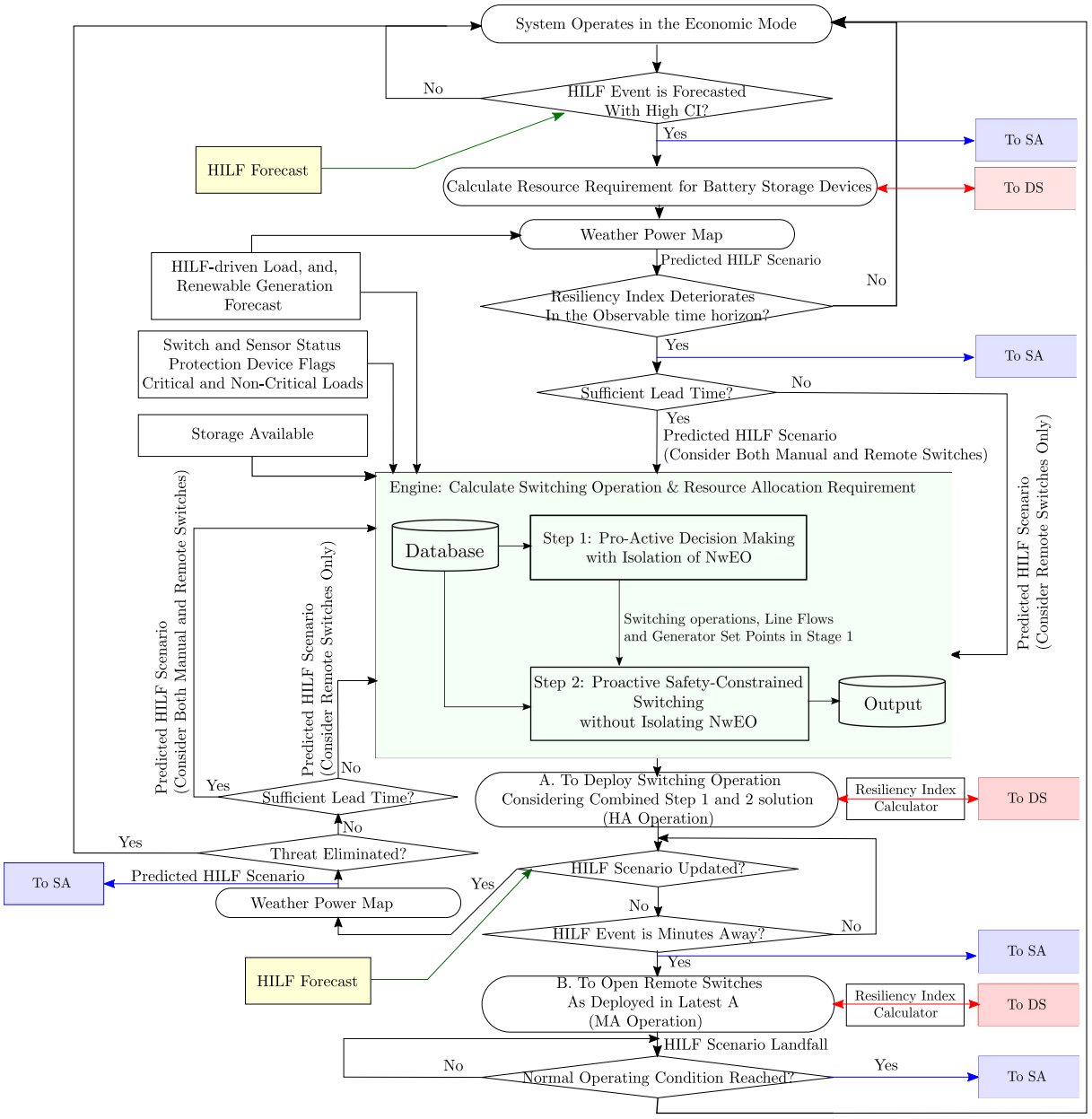

FIGURE 2. **Proactive network switching and resource allocation framework with dataflow. Region shaded in green constitutes the proposed algorithm and the focus of this paper. Boxes marked in blue, red and yellow are for SA, DS and external forecast module respectively.**

would continue to operate economically unless the associated HILF impact is visible in the DSO observable time horizon. The entire decision-making framework, along with the landmark points where the DSO interacts with the proposed algorithm, is provided in Fig. 2, which is expanded from the framework provided in [28].

If the HILF event is forecasted with high CI and the resiliency index deteriorates within the DSO's observable time horizon, the DSO would be provided with information about the looming threat through the SA mechanism and associated performance analysis (see Fig. 1). Multiple resiliency indices with varying details exist in the literature to identify the implications of these events [28], [33]. We utilize the indices given in our earlier research [34] (not explicitly shown here for brevity), which relies on (i) the topological robustness of the PDS, (ii) the extent of the failure of the system given prior experience, (iii) the capacity to serve CLs in the face of additional failures, (iv) CL demand actually served, and (v) resource available from DGs and BSDs. If the forecast is beyond a specific CI and the resiliency score as a part of the performance analysis tool within the RMS deteriorates, the proposed two-stage methodology will be automatically invoked. Here, the DSO would consider halting the market operation and switch to resiliency mode.

Subsequently, the SA signal is sent to the operator to remain alert. The metric is suitably adapted to work with the forecasted event and will be utilized to provide the operator with the what-if analysis of the system condition (with and without deployment of resiliency improvement measures).

Possible DS for the DSO relies on two major factors, (i) resource availability and (ii) available lead time for crew dispatch. As already indicated, given high uncertainty regarding the landfall of HILF events, crew deployment to operate some of the MO switches to reconfigure the system or deenergize a part of the system as the situation demands get severely limited. Nevertheless, available infrastructure resources in terms of deployed smart sensors and monitoring devices at desirable locations facilitate monitoring the system in real-time, facilitating the operation of some of the RO switches. As shown in Fig. 1, the proposed algorithm is capable of being integrated with an external forecaster through a power-weather translation map in SCADA, while various sensor statuses, D-PMUs, AMI information, storage status, along with locations of CLs are also available in SCADA. Given typical load and generation forecasts may not be reasonable enough[3] HILF-driven forecasts will be utilized.

Given the supplied information, the proposed optimization engine will calculate: (i) switching strategy (for both MO and RO switches), (ii) desired set-points allocation for the DGs, and (iii) resource allocation for the BSDs for the discussed Stage 1 and Stage 2 within the observable operating horizon for the DSO. As discussed, combined Stage 1 and 2 outputs will be provided to the DSO as DS for HA deployment. Here, the DSO will also be provided with the resiliency metric for the observable period and a what-if scenario utilizing the resiliency metric if the proposed DS is not deployed (see Fig. 6 for an example and associated discussion). The system status will be continuously monitored for any change in the forecast. Depending on the lead time and current system operating condition, the DSO will be periodically provided the necessary DS and SA if the forecast evolves. Notably, if the threat vanishes with significant CI at any point, the system would move to economic mode, and the alert status would be removed. Else, once the HILF event is minutes away, as discussed, the RO-operated switches determined in Stage 2 would be opened to isolate the NwEO. Given switching requirements for both Stage 1 and 2 were calculated to facilitate HA deployment, real-time computation needs would be completely alleviated, especially with mixed-integer problem formulation. As discussed in Section III-B, appropriate linearization strategies are available in the literature to convert it into a mixed-integer linear program (MILP). While the scope of proactive reconfiguration ends here, continuous monitoring and corrective reconfiguration will be pursued until the treats are completely eliminated, which is the scope of another paper.

Notably, the SA mechanism is utilized to alert the system operator, and therefore the information flow is unidirectional, while the DS mechanism relies on operator feedback to execute the control actions, making the information flow bidirectional.

B. CONSTRAINTS LINEARIZATION TECHNIQUES OF THE OPTIMIZATION PROBLEM

The nonlinear equations in the problem formulation can be divided into three major categories discussed as follows:

1) CONNECTIVITY CONSTRAINTS

The primary focus here is to linearize the product of a binary and an integer variable. For example, one may refer to eq. 6. Suppose, $\mathcal{Z}_{i,j} = z_{i,j}\left(V_i - V_j + \epsilon\right)$, then this variable can be linearized using big-M method as follows:

$$-|N| \leq \mathcal{Z}_{i,j} \leq |N| \tag{51}$$

$$-|N|\, z_{i,j} \leq \mathcal{Z}_{i,j} \leq |N|\, z_{i,j} \tag{52}$$

$$\begin{aligned} V_i - V_j + \epsilon - (1 - z_{i,j})\,|N| &\leq \mathcal{Z}_{i,j} \\ &\leq V_i - V_j + \epsilon + (1 - z_{i,j})\,|N| \end{aligned} \tag{53}$$

Here, $|N|$ represents the number of nodes within the PDS. Notably, if $\epsilon = 1$, it is notable that $\left(V_i - V_j + \epsilon\right)$ would be limited by $|N|$. Furthermore, suitably chosen big-M helps ensure faster convergence of the optimization problem.

2) LINE FLOW CONSTRAINTS

Next consider a polygon enclosed within a circle is constituted of $\mathbb{W}$ equal segments, then the corner points lying on the circle of radius $|\mathbb{V}|$ can be given by $(|\mathbb{V}|, 0)$, $\left(|\mathbb{V}|\cos\left(\frac{2\pi}{\mathbb{W}}\right), |\mathbb{V}|\sin\left(\frac{2\pi}{\mathbb{W}}\right)\right), \cdots, \left(|\mathbb{V}|\cos\left(\frac{2\pi(\mathbb{W}-1)}{\mathbb{W}}\right), |\mathbb{V}|\sin\left(\frac{2\pi(\mathbb{W}-1)}{\mathbb{W}}\right)\right)$. Given any two adjacent corner points, $\left(V_\mathrm{p}, W_\mathrm{p}\right)$ and $\left(V_\mathrm{q}, W_\mathrm{q}\right)$, and supposing, (V, W) be an arbitrary point lying on the polygon approximate, the segment representing the linear approximation can be given by,

$$V\left(W_\mathrm{q} - W_\mathrm{p}\right) + W\left(V_\mathrm{p} - V_\mathrm{q}\right) = \left(V_\mathrm{p}W_\mathrm{q} - W_\mathrm{p}V_\mathrm{q}\right) \tag{54}$$

Suitably chosen $(V_\mathrm{p}, W_\mathrm{p})$, $(V_\mathrm{q}, W_\mathrm{q})$ will result in $(V_\mathrm{p}W_\mathrm{q} - W_\mathrm{p}V_\mathrm{q}) \geq 0$, for each segment of the polygon approximation. Now, suppose, (V, W) to be an arbitrarily chosen point on the associated two-dimensional space. Because the common region needs to contain $(0, 0)$, polygonal inner approximates can be given by,

$$V\left(W_\mathrm{q} - W_\mathrm{p}\right) + W\left(V_\mathrm{p} - V_\mathrm{q}\right) \leq \left(V_\mathrm{p}W_\mathrm{q} - W_\mathrm{p}V_\mathrm{q}\right);\ \forall \mathrm{p}, \mathrm{q} \tag{55}$$

3) VOLTAGE CONTROL NODE REQUIREMENTS

The Big-M method is applied for linearizing the product of a binary and a continuous variable. Equation (30) is one such equation that includes the product of a binary

[3]Two examples can be referred to here: (i) lack of weatherization led to outage of several power plants during Texas power outage in 2021 [2], (ii) heatwave, especially during wildfire events, would lead to extreme air conditioning requirements, which generally do not get captured in traditional forecasters.

and a continuous variable, which is also similar to the product of a binary and integer variables. Consider $\mathcal{Y}_i^t = \left(1 - \sum_{\forall j:(i,j)\in W} z_{j,i}\right)\left(v_i^t - v^{ref}\right)$, then we can linearize this variable as follows:

$$-\Delta v^{\max} \leq \mathcal{Y}_i^t \leq \Delta v^{\max} \tag{56}$$

$$-\Delta v^{\max}\left(1 - \sum_{\forall j:(i,j)\in W} z_{j,i}\right) \leq \mathcal{Y}_i^t \leq \Delta v^{\max}\left(1 - \sum_{\forall j:(i,j)\in W} z_{j,i}\right) \tag{57}$$

$$v_i^t - v^{ref} - \sum_{\forall j:(i,j)\in W} z_{j,i}\Delta v^{\max} \leq \mathcal{Y}_i^t \leq v_i^t - v^{ref} + \sum_{\forall j:(i,j)\in W} z_{j,i}\Delta v^{\max} \tag{58}$$

Here, $\Delta v^{\max}$ is suitably chosen so that $-\Delta v^{\max} \leq v_i^t - v^{ref} \leq \Delta v^{\max}$.

IV. TEST SYSTEMS AND SIMULATION RESULTS

The proposed framework has been tested and validated on a modified IEEE 123-node test system and a real-world 45-node isolated μ-grid model based on the CEC Alaska system. The location of MO and RO switches for both the modified IEEE 123-node test system and 45-node μ-grid are shown in Figs. 4 and 5. Here, the nodes and the lines within the region identified by A (dark gray region) are expected to face catastrophe, and with the limited availability of RO switches, all the nodes within region B (light gray part) will be required to be isolated; defining the NwEO. Locations of local DGs and BSDs, along with CLs and NCLs, are also provided. The CLs and NCLs are connected via AMI switches and are individually and remotely controllable to ensure load-generation balance with limited resource availability. All the DGs and BSDs are equipped with anti-islanding protection, where they will be automatically de-energized upon realizing the absence of a healthy network or inputs from a μ-grid controller. All the BSDs have charging and discharging efficiencies of 0.95 and 0.90, respectively. This paper assumes that appropriate relays are located throughout the PDS (especially across both RO and MO switches) for seamless disconnection and re-connection of μ-grids according to IEEE 1547-2018 standards.

For analysis, it is assumed that the values of the served loads remain similar at every node at 100 and 10, respectively, for the critical and non-critical counterparts. It is considered that the entire PDS remains under the hazardous zone, with eight intervals of equal duration being the DSO observable time horizon with a longevity of 15 minutes each. Given the uncertainty of the HILF events, the crews won't be deployed if the event is three intervals away. We assume the availability of an adequate number of operational crews, facilitating a quick deployment of MO switches.

A. RESILIENCY METRIC EVALUATION

Given the HILF event forecast, the following three scenarios are considered in this paper to evaluate the efficacy of our proposed methodology:

i. the proposed reconfiguration strategy is not deployed with NwEO isolated minutes before;
ii. the PDS is proactively reconfigured, and only switching actions depicted in Stage 1 is deployed as HA operation (NwEO are de-energized well before the disaster strikes); and hence, the healthy section of the PDS remains unharmed following the disaster; and
iii the PDS operates according to the proposed strategy (see Fig. 2). Switching actions are periodically reviewed with the propagation of disaster events, while the closed switches determined at the second stage are opened minutes before the event's arrival.

The resiliency index of the system for all the three scenarios is given in Fig. 3 for both the considered IEEE modified 123-node test system and 45-node real-world test system. The switching requirements of the PDS are presented in Figs. 4 and 5 respectively. The underlying two-stage optimization problem converges within $\approx 250s$ (with a Core-i7 processor and 32 GB of RAM), indicating the real-world deployability of the proposed algorithm.

As seen from the figure, in scenario (i), the resiliency index of the PDS remains very high until the disaster strikes. The limited RO switches with no preparation reduce the associated index to a meager value following the arrival of the disaster. In scenario (ii), prior reconfiguration drives the post-disaster resiliency index to a very high value. However, earlier de-energization of the NwEO reduces the pre-event resiliency index significantly. The post-disaster performance in scenario (iii) is similar to scenario (ii). Partial survival of NwEO in the pre-event operation leads the resiliency index to remain higher than that of scenario (ii). However, limited local generation availability and no flow requirement from the healthy part to NwEO enforces that only a partial set of CLs will be served, resulting in a lower resiliency index than the no-action scenario (scenario i).

B. SWITCHING AND RESOURCE ALLOCATION STRATEGY FOR MODIFIED IEEE 123 NODE DISTRIBUTION NETWORK

Here, as a part of the economic operation, switches 13-152, 18-135, 54-94, 97-197, and 61-610 in Fig. 4 operate in a normally closed mode. An alternative path to a CL at 610 of $245\angle$-36.30° kW is also available through a line of the capacity of 200 kVA. A BSD is also available at node 610. The HILF scenario is assumed to damage the energized lines and nodes as shown in the dark grey shaded region (region A) in Fig. 4. If the system was operating in economic mode when the disaster strikes, all the CL connected at nodes 65, 114, and 76 will experience outages. CL at node 610 won't suffer any outages with make-before-break switching.

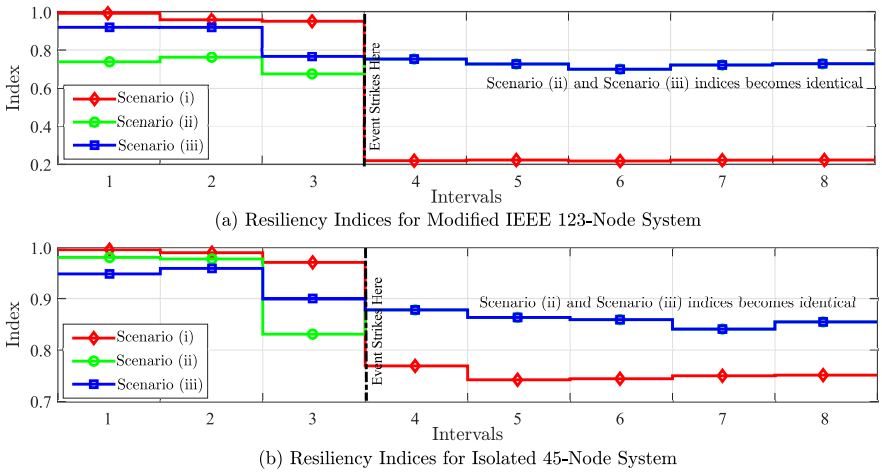

(a) Resiliency Indices for Modified IEEE 123-Node System

(b) Resiliency Indices for Isolated 45-Node System

FIGURE 3. **Varying resiliency metric with proactive control.**

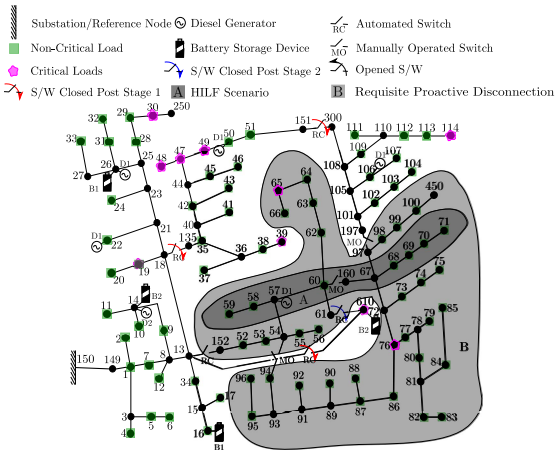

FIGURE 4. **Optimally reconfigured modified IEEE 123-node test system.**

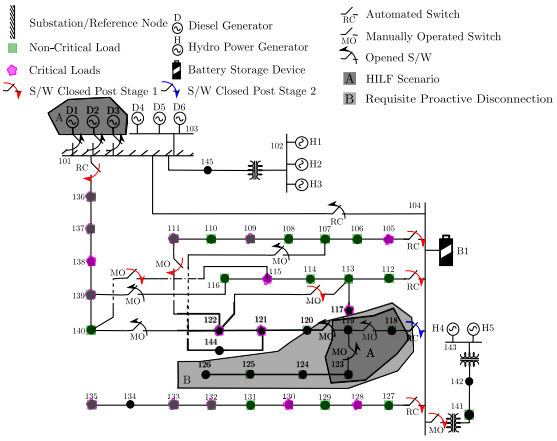

FIGURE 5. **Optimally reconfigured modified isolated μ-grid as proactive measure.**

Alternatively, with the two-stage algorithm, the efficacy of Stage 1 is also shown in Fig. 4, where CLs at nodes 114 and 610 will continue to be served during the contingency due to proactive control actions. It is important to note that the limited transmission corridor between 13-610 and the finiteness of the energy stored within the BSD imposes additional challenges to serving the associated CL. The switching action required in Stage 2 of the problem is also provided. Here, remotely operable switches 61-610 remain closed until disaster strikes, allowing survival of the NwEO in case the HILF forecasts change significantly. While the flow through the corresponding switch remains at zero, the availability of the DG at node 57 ensures that the CL at node 65 is served until disaster strikes. Unavailability of local generation dictates that CL at 76 will not be served.

C. SWITCHING AND RESOURCE ALLOCATION STRATEGY FOR ISOLATED 45-NODE REAL WORLD CEC μ-GRID

Here, we consider that lines 101-104, 101-136, 104-105, 104-112, 104-118, 104-127, and 104-141 are normally closed during economic operation mode. Here, the HILF scenario is predicted to disrupt nodes 118, 119, and 123. Generators D1, D2, and D3 are also considered to be in the path of disaster (in a realistic scenario, such as a snow avalanche). In this configuration, without proactive control, not only CLs at nodes 121 and 122 will be disrupted following the event, but the traditional practices also recognize that the event-stricken energized DGs usually suffer severe damages, resulting in post-disaster delayed recovery.

It is apparent that, through proactive control, the CLs at nodes 121 and 122 can be supplied through an alternative route (see Fig. 5). Since most of the lines available for reconfiguration are manually operated, the proactive control gains immense significance in this case. Additionally, since the shed region has no local generation, none of the loads can be served during the contingencies. To alleviate this issue and demonstrate the efficacy of the proposed algorithm, we allow the power to flow through remotely operable switches. Consequently, we observed that node 118 remains live until minutes before disaster strikes, and the NCLs at node 118 is

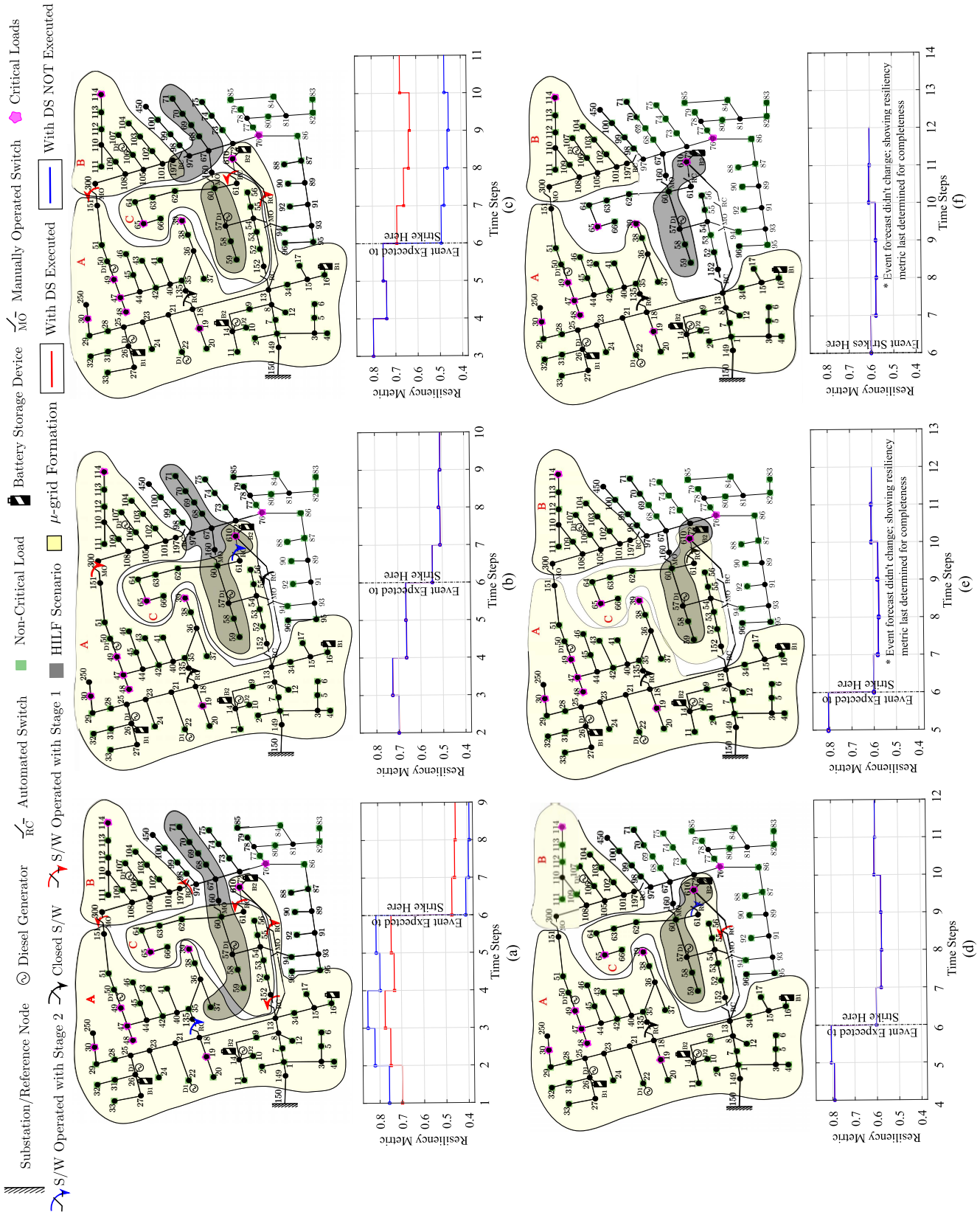

FIGURE 6. DS provided to operate the grid as multi-μ-grid system as the weather event progresses. (a) → (b) → (c) → (d) → (e) → (f).

still served. However, since the rest of the affected nodes are connected via manual switches, those nodes will remain de-energized until the disaster dissipates.

D. SWITCHING AND RESOURCE ALLOCATION STRATEGY WITH PROGRESSING WEATHER EVENT

Given that the HILF events are highly unpredictable, the operators would have to often operate with limited CI in the prediction. Furthermore, limited lead-time for safe deployment of crews also affects some of the decision-making, as shown in Fig. 2. As discussed, with evolving HILF event and possible affected regions, the PDS would be required to be continuously reconfigured until the event materializes. The DSO would be provided with the reconfiguration strategy and the resiliency metric for the time interval based on which the metric was calculated.

The efficacy of the algorithm is shown in Fig. 6, where the reconfiguration strategy along with μ-grid formation, along with the resiliency with and without deployment of the proposed DS is depicted, which will ultimately be provided to the DSO as DS.[4] As shown in the figure, the HILF scenario is revised in time steps 1, 2, 3, and 4, which could be obtained from established ML-based outage predictors. Given the assumption that an adequate number of crew is available, manual switching operations could be carried out instantly, and crews will not be deployed if the disaster is three time steps away. Note that DS won't be provided if no changes are reported in the HILF forecaster, and ADMS would assume generation control.

As shown in Fig. 6(a), given the HILF scenario, three networked μ-grids, namely, A, B, and C, are expected to form. Given node 37 is expected to be a NwEO, the MO switch between nodes 151-300 remains open, and μ-grid B is operated in islanded mode. NwEO will be isolated if the said HILF event materializes with RO switch between nodes 18-135. However, if the proposed DS strategy was not executed, although the ability to serve a majority of the loads would result in a high enough pre-event metric, which gets significantly lowered following the occurrence of the disaster. As illustrated in Fig. 6(b), at time step 2, the threat at NwEO 37 is projected to get eliminated, but node 610 is shown to be a NwEO. Given the current configuration, since the NwEOs can be isolated through remote switches, resiliency metric with and without reconfiguration remains similar. Here, node 610 was isolated with the associated remote switch, and MO switch between nodes 151-300 has been closed given sufficiently available lead time. While the closing of the MO switch would lead to μ-grid B no longer operating in isolation, this has no significant impact on the resiliency metric. Subsequently, as depicted in Fig. 6(c), the HILF event is predicted to evolve, and node 197 is now expected to be a NwEO, prompting crew deployment to open the closed MO switch between nodes 151-300. Here, μ-grid B would operate in islanded mode and would be deenergized if the HILF materializes. Notably, if the MO switch is not opened, nodes 47, 48, and 49 containing CLs would have to be deenergized, significantly reducing the resiliency metric.

HILF event was further revised in the subsequent time step, prompting μ-grid B to be no more under threat. However, given the available lead time, the crew to operate the MO switch won't be deployed, and μ-grid B would continue to operate as islanded. Given the threatened region could be isolated through RO switches, the reconfiguration strategy as DS has no impact on the resiliency metric. The threat forecast didn't change for the next two intervals. Notably, RO switches between nodes 13-152 remained open to operate μ-grid C as islanded and will be deenergized as shown in Fig. 6(f). Furthermore, CL at node 76 would remain undelivered given the absence of local DGs. Notably, the scope of the proposed proactive controller is limited to the landfall of the HILF event.

V. CONCLUSION

A two-stage proactive network switching and resource allocation strategy for supply continuity to the CLs during HILF events has been proposed in this work. The proposed algorithm relies on external early event warnings and HILF forecasts to proactively de-energize a part of the PDS, reducing risks for system impact caused by the unplanned outage of live components as the event propagates, with possible faster recovery following the event. Here, the operational crews are dispatched to configure both manually and remotely operable switches for the maximal value of the load being served hours before the event while further maximizing it by allowing the loads to remain energized minutes before the event strikes. Along with network switching and resource allocation strategy, the operator is provided with the benefits of deployment of the suggested strategy through a resiliency metric. The provision of continuous rectification with progressing HILF events is also considered. The developed mathematical model is demonstrated to ensure radiality while isolating healthy parts from nodes with expected outage (NwEO), possibly forming multiple isolated μ-grids. The utility of the proposed strategy is demonstrated through a modified IEEE 123-node network and an isolated 45-node real-world microgrid in Alaska, considering realistic case scenarios. Compared to solely proactive isolation and switching, the strength of the proposed strategy is demonstrated. Interactive situational assessment and decision support would significantly help the operator, especially during stressful operating conditions as the HILF event progresses. The robustness and scalability of the proposed resiliency strategy are significant improvements to traditional HILF emergency response. The proposed framework could be expanded to real-world scenarios with limited crew availability and road situations, and possible delays in the deployment of the control strategy. Uncertainty in the system-wide load demand could also be judiciously incorporated.

[4]Here, we assume that DSO deploys the suggested DS, and is used to calculate the resiliency metric if the said DS is not deployed for the next time step.

ACRONYMS

Acronyms used in this paper are tabulated below:

ADMS	Advanced Distribution Management System.
AMI	Advanced Metering Infrastructure.
BSDs	Battery Storage Devices.
CEC	Cordova Electric Cooperative.
CI	Confidence Interval.
CLs	Critical Loads.
D-PMU	Distribution-level Phasor Measurement Unit.
DERs	Distributed Energy Resources.
DGs	Diesel Generators.
DS	Decision Support.
DSOs	Power Distribution System Operators.
HA	Hours Ahead.
HILF	High-Impact Low Frequency.
IBRs	Inverter-based Resources.
ICTs	Information and Communication Technology.
MA	Minutes ahead (operation).
MILP	Mixed-Integer Linear Program.
MO	Manually Operable (switch).
NCLs	Non-critical Loads.
NwEO	Nodes with Expected Outages.
PDS	Power Distribution Systems.
RMS	Resiliency Management System.
RO	Automated/remotely Operable (switch).
SA	Situational Awareness.
SCADA	Supervisory Control and Data Acquisition.

ACKNOWLEDGMENT

The authors would like to thank Dr. R. Hovsapian, Dr. M. Panwar, and Dr. S. Pannala for all the technical support.

REFERENCES

[1] *Billion-Dollar Weather and Climate Disasters: Table of Events*, Nat. Centers Environ. Inf., Asheville, North Carolina, 2016.

[2] B. Storrow. *Why the Deep Freeze Caused Texas to Lose Power*. [Online]. Available: https://www.scientificamerican.com/article/why-thedeep-freeze-caused-texas-to-lose-power/

[3] Y. Xu, C.-C. Liu, K. P. Schneider, F. K. Tuffner, and D. T. Ton, "Microgrids for service restoration to critical load in a resilient distribution system," *IEEE Trans. Smart Grid*, vol. 9, no. 1, pp. 426–437, Jan. 2016.

[4] W. C. Edwards, S. Manson, and J. Vico, "Microgrid islanding and grid restoration with off-the-shelf utility protection equipment," in *Proc. IEEE Canada Int. Humanitarian Technol. Conf. (IHTC)*, Jul. 2017, pp. 188–192.

[5] T. Fenimore, A. Gould, and L. Wright, "Implementing a microgrid using standard utility control equipment," in *Proc. 70th Annu. Conf. Protective Relay Engineers (CPRE)*, Apr. 2017, pp. 1–9.

[6] J. Li, X.-Y. Ma, C.-C. Liu, and K. P. Schneider, "Distribution system restoration with microgrids using spanning tree search," *IEEE Trans. Power Syst.*, vol. 29, no. 6, pp. 3021–3029, Nov. 2014.

[7] Boston Consulting Group. (2020). *Sentient Energy's Grid Analytics System Moves the Needle on Wildfire Mitigation & Emergency Response Initiatives*. [Online]. Available: http://sentientenergy.com/wp-content/uploads/2021/06/Sentient-Energy-Wildfire-Public-Safety-Solution.pdf

[8] Utility Dive's Brand Studio. *In Any Weather: Enhance Outage Prediction and Prevention With Artificial Intelligence*. Accessed: May 4, 2022. [Online]. Available: https://www.ibm.com/downloads/cas/70BARQZ6

[9] Z. Wang. (2019). *How Artificial Intelligence and Advanced Optimization Help Improve Outage Management—IEEE Smart Grid*. [Online]. Available: https://smartgrid.ieee.org/bulletins/september-2019/howartificial-intelligence-and-advanced-optimization-help-improve-outagemanagement

[10] J. Xie, I. Alvarez-Fernandez, and W. Sun, "A review of machine learning applications in power system resilience," in *Proc. IEEE Power Energy Soc. Gen. Meeting (PESGM)*, Aug. 2020, pp. 1–5.

[11] M. A. Mohamed, T. Chen, W. Su, and T. Jin, "Proactive resilience of power systems against natural disasters: A literature review," *IEEE Access*, vol. 7, pp. 163778–163795, 2019.

[12] C. Ji, Y. Wei, H. Mei, J. Calzada, M. Carey, S. Church, T. Hayes, B. Nugent, G. Stella, M. Wallace, J. White, and R. Wilcox, "Large-scale data analysis of power grid resilience across multiple us service regions," *Nature Energy*, vol. 1, no. 5, pp. 1–8, May 2016.

[13] A. Arab, A. Khodaei, Z. Han, and S. K. Khator, "Proactive recovery of electric power assets for resiliency enhancement," *IEEE Access*, vol. 3, pp. 99–109, 2015.

[14] H. Gao, Y. Chen, S. Mei, S. Huang, and Y. Xu, "Resilience-oriented pre-hurricane resource allocation in distribution systems considering electric buses," *Proc. IEEE*, vol. 105, no. 7, pp. 1214–1233, Jul. 2017.

[15] G. Huang, J. Wang, C. Chen, J. Qi, and C. Guo, "Integration of preventive and emergency responses for power grid resilience enhancement," *IEEE Trans. Power Syst.*, vol. 32, no. 6, pp. 4451–4463, Nov. 2017.

[16] A. Gholami, T. Shekari, F. Aminifar, and M. Shahidehpour, "Microgrid scheduling with uncertainty: The quest for resilience," *IEEE Trans. Smart Grid*, vol. 7, no. 6, pp. 2849–2858, Nov. 2016.

[17] A. Hussain, V.-H. Bui, and H.-M. Kim, "A proactive and survivability-constrained operation strategy for enhancing resilience of microgrids using energy storage system," *IEEE Access*, vol. 6, pp. 75495–75507, 2018.

[18] C. Wang, S. Lei, P. Ju, C. Chen, C. Peng, and Y. Hou, "MDP-based distribution network reconfiguration with renewable distributed generation: Approximate dynamic programming approach," *IEEE Trans. Smart Grid*, vol. 11, no. 4, pp. 3620–3631, Jul. 2020.

[19] D. N. Trakas and N. D. Hatziargyriou, "Optimal distribution system operation for enhancing resilience against wildfires," *IEEE Trans. Power Syst.*, vol. 33, no. 2, pp. 2260–2271, Mar. 2017.

[20] M. Panteli, D. N. Trakas, P. Mancarella, and N. D. Hatziargyriou, "Boosting the power grid resilience to extreme weather events using defensive islanding," *IEEE Trans. Smart Grid*, vol. 7, no. 6, pp. 2913–2922, Nov. 2016.

[21] S. Pandey, S. Chanda, A. K. Srivastava, and R. O. Hovsapian, "Resiliency-driven proactive distribution system reconfiguration with synchrophasor data," *IEEE Trans. Power Syst.*, vol. 35, no. 4, pp. 2748–2758, Jul. 2020.

[22] (2010). *CA-LNU-Bodega Bay—Wildland Fire—98 Acres—100% #Wildfire*. [Online]. Available: https://calfire.blogspot.com/2010/09/ca-lnu-bodegabay-wildland-fire-89.html

[23] J. T. Abatzoglou, C. M. Smith, D. L. Swain, T. Ptak, and C. A. Kolden, "Population exposure to pre-emptive de-energization aimed at averting wildfires in northern California," *Environ. Res. Lett.*, vol. 15, no. 9, Sep. 2020, Art. no. 094046.

[24] Y. Wang, C. Chen, J. Wang, and R. Baldick, "Research on resilience of power systems under natural disasters—A review," *IEEE Trans. Power Syst.*, vol. 31, no. 2, pp. 1604–1613, Mar. 2016.

[25] S. Lei, C. Chen, Y. Song, and Y. Hou, "Radiality constraints for resilient reconfiguration of distribution systems: Formulation and application to microgrid formation," *IEEE Trans. Smart Grid*, vol. 11, no. 5, pp. 3944–3956, Sep. 2020.

[26] H. Farzin, M. Fotuhi-Firuzabad, and M. Moeini-Aghtaie, "Enhancing power system resilience through hierarchical outage management in multi-microgrids," *IEEE Trans. Smart Grid*, vol. 7, no. 6, pp. 2869–2879, Nov. 2016.

[27] C. Lin, C. Chen, F. Liu, G. Li, and Z. Bie, "Dynamic MGs-based load restoration for resilient urban power distribution systems considering intermittent RESs and droop control," *Int. J. Electr. Power Energy Syst.*, vol. 140, Sep. 2022, Art. no. 107975.

[28] G. Kandaperumal, S. Majumder, and A. K. Srivastava, "Microgrids as a resilience resource in the electric distribution grid," in *Electric Power Systems Resiliency Modelling, Opportunity and Challenges*. Amsterdam, The Netherlands: Elsevier, 2022.

[29] P. Pederson, D. Dudenhoeffer, S. Hartley, and M. Permann, "Critical infrastructure interdependency modeling: A survey of us and international research," *Idaho Nat. Lab.*, vol. 25, p. 27, Aug. 2006.

[30] S. Poudel and A. Dubey, "Critical load restoration using distributed energy resources for resilient power distribution system," *IEEE Trans. Power Syst.*, vol. 34, no. 1, pp. 52–63, Jan. 2019.
[31] J. A. Taylor and F. S. Hover, "Convex models of distribution system reconfiguration," *IEEE Trans. Power Syst.*, vol. 27, no. 3, pp. 1407–1413, Aug. 2012.
[32] M. E. Baran and F. F. Wu, "Network reconfiguration in distribution systems for loss reduction and load balancing," *IEEE Trans. Power Del.*, vol. 4, no. 2, pp. 1401–1407, Apr. 1989.
[33] G. Kandaperumal and A. K. Srivastava, "Resilience of the electric distribution systems: Concepts, classification, assessment, challenges, and research needs," *IET Smart Grid*, vol. 3, no. 2, pp. 133–143, Apr. 2020.
[34] G. Kandaperumal, S. Pandey, and A. Srivastava, "AWR: Anticipate, withstand, and recover resilience metric for operational and planning decision support in electric distribution system," *IEEE Trans. Smart Grid*, vol. 13, no. 1, pp. 179–190, Jan. 2022.

SUBIR MAJUMDER (Member, IEEE) received the Ph.D. degree under a Cotutelle/Joint Agreement between the Indian Institute of Technology Bombay, India, and the University of Wollongong, Australia, in 2020.

From 2020 to 2021, he worked as a Postdoctoral Research Associate at Washington State University, Pullman, WA, USA. He is currently working as an Engineering Scientist at the Lane Department of Computer Science and Electrical Engineering, West Virginia University, Morgantown, WV, USA. His research interests include power systems modeling, operations (including operational resiliency) and planning, power system economics, distributed optimization, power quality, and smart grid. He was conferred the POSOCO Power System Awards (PPSA) under Doctoral Category in 2020.

GOWTHAM KANDAPERUMAL (Member, IEEE) received the master's degree in electrical engineering from Arizona State University, in 2014, and the Ph.D. degree in electrical engineering and computer science from Washington State University, in 2021. He is currently a Senior Engineer with Commonwealth Edison (ComEd), Chicago, IL, USA, working with the Reliability Group. Prior to ComEd, he was a Distinguished Graduate Research Fellow at the Pacific Northwest National Laboratory (2019–2021) and an Electrical Engineer at Affiliated Engineers Inc. (2014–2017).

SHIKHAR PANDEY (Member, IEEE) received the bachelor's degree in electrical engineering from the National Institute of Technology, Patna, in 2013, and the M.S. and Ph.D. degrees in electrical engineering from Washington State University, Pullman, in 2017 and 2020, respectively.

From 2013 to 2015, he worked as a Senior Electrical Engineer with Larsen and Toubro ECC, Kullu, India. He is currently a Principal Quantitative Engineer with the DER Engineering Group, Commonwealth Edison. His research interests include microgrids, smart grids, planning and operations, and synchrophasor technology and its applications.

ANURAG K. SRIVASTAVA (Fellow, IEEE) received the Ph.D. degree in power engineering from the Illinois Institute of Technology, Chicago, IL, USA, in 2005.

He is currently a Raymond J. Lane Professor and the Chairperson with the Computer Science and Electrical Engineering Department, West Virginia University. He is also an Adjunct Professor with the Washington State University and a Senior Scientist with the Pacific Northwest National Laboratory. He is the author of more than 300 technical publications, including a book on power system security and four patents. His research interests include data-driven algorithms for power system operation and control including resiliency analysis.

Prof. Srivastava is serving as the Chair for the PES Voltage Stability Working Group and the Vice-Chair for the Power System Operation Sub-Committee, and the Vice-Chair of Tools for Power Grid Resilience Task Force.

CLAY KOPLIN (Member, IEEE) received the B.S. degree in electrical engineering from the University of Alaska Fairbanks, Fairbanks, AK, USA, in 1992, and the M.B.A. degree in strategic management and corporate structure from the Indiana University Bloomington–Kelley School of Business M.B.A. Program.

From 1992 to 1998, he worked as a Staff Engineer at the Kodiak Electric Association, Kodiak, AK, USA, and from 1998 to 2007, he was a Manager of engineering & operations at Cordova Electric Cooperative, Cordova, AK, USA. He is currently working as the CEO of Cordova Electric Cooperative.